

Magnetized accretion disks around Kerr black holes with scalar hair - I. Constant angular momentum disks

Sergio Gimeno-Soler,¹ José A. Font,^{1, 2} Carlos Herdeiro,³ and Eugen Radu³

¹*Departamento de Astronomía y Astrofísica, Universitat de València,
C/ Dr. Moliner 50, 46100, Burjassot (València), Spain*

²*Observatori Astronòmic, Universitat de València,
C/ Catedrático José Beltrán 2, 46980, Paterna (València), Spain*

³*Departamento de Física da Universidade de Aveiro and CIDMA, Campus de Santiago, 3810-183 Aveiro, Portugal*

(Dated: November 6, 2018)

Testing the true nature of black holes – the no-hair hypothesis – will become increasingly more precise in the next few years as new observational data is collected in both the gravitational wave channel and the electromagnetic channel. In this work we consider numerically generated spacetimes of Kerr black holes with synchronised scalar hair and build stationary models of magnetized constant angular momentum thick disks around them. We study the dependence of the morphology and properties of the accretion tori on the type of black hole considered, from purely Kerr black holes with varying degrees of spin parameter to Kerr black holes with scalar hair with different ADM mass and horizon angular velocity. **TF: To be completed.**

PACS numbers: 95.30.Sf, 04.70.Bw, 04.40.Nr, 04.25.dg

I. INTRODUCTION

In recent years, new families of stationary, asymptotically flat black holes (BHs) avoiding the so-called “no hair” theorems, have been obtained both in general relativity and modified gravity (see e.g. [1] and references therein). Among those, Kerr BHs with synchronised hair [2, 3] are a counterexample to the no hair conjecture resulting from minimally coupling Einstein’s gravity to simple (bosonic) matter fields obeying all energy conditions. The physical conditions and stability properties of these classes of *hairy* BHs (HBHs) have been recently investigated to assess their potential viability as alternatives to astrophysical Kerr BHs. On the one hand, Kerr BHs with Proca hair have been shown to form dynamically as the end-product of the superradiant instability [4, 5] (see also [6, 7] for the case of a charged scalar field around a charged BH in spherical symmetry). On the other hand, the stability of these solutions, questioned by [8] in the scalar case, has been recently revisited by [9] who have shown that the domain of HBH solutions for which the superradiant instability might affect their actual existence has no significance for astrophysical BHs, rendering HBHs as *effectively* stable.

In the observational arena, the LIGO/Virgo detection of gravitational waves from binary BHs [10–14] and the exciting prospects of observing the first image – the black hole *shadow* – of a BH by the Event Horizon Telescope (EHT) [15] opens the opportunity to test the true nature of BHs – the no-hair hypothesis – and, in particular, the astrophysical relevance of HBHs. It is not yet known whether the LIGO/Virgo binary BH signals are consistent with alternative scenarios, such as the merger of ultracompact boson stars or non-Kerr BHs, because the latter possibilities remain thus far insufficiently modelled. Likewise, Kerr BHs with scalar hair (KBHsSH) can exhibit very distinct shadows from those of (bald) Kerr

BHs, as shown by [16] and [17] for two different setups for the light source, either a celestial sphere far from the compact object or an emitting torus of matter surrounding the BH, respectively. It is therefore an intriguing open possibility if the very long baseline interferometric observations of BH candidates in Sgr A* and M87 envisaged by the EHT may constrain the astrophysical significance of HBHs.

The setup considered by [17] in which the light source producing the BH shadow is an accretion disk, is arguably more realistic than the distant celestial sphere of [16]. Thick accretion disks (or tori) are common systems in astrophysics, either surrounding the supermassive central BHs of quasars and active galactic nuclei or, at stellar scale, surrounding the compact objects in X-ray binaries, microquasars, and gamma-ray bursts (see [18] and references therein). In this paper we present new families of stationary solutions of magnetized thick accretion disks around KBHsSH that differ from those considered by [17]. Our procedure, which combines earlier approaches put forward by [19, 20] was presented in [21] for the Kerr BH case. In Ref. [21] we built equilibrium sequences of accretion disks in the test-fluid approximation endowed with a purely toroidal magnetic field, assuming a form of the angular momentum distribution that departs from the constant case considered by [19] and from which the location and morphology of the equipotential surfaces can be numerically computed. Our goal in the present work is to extend this approach to KBHsSH and to assess the dependence of the morphology and properties of accretion disks on the type of BH considered, either Kerr BHs of varying spins or KBHsSH. In this investigation we focus on disks with a constant distribution of specific angular momentum, presenting in a companion paper the non-constant (power-law) case, whose sequences have already been computed. The dynamical stability of these solutions as well as the analysis of the

corresponding shadows will be discussed elsewhere.

The organization of this paper is as follows: Section II presents the mathematical framework we employ to build magnetized disks in the numerically generated space-times of KBHsSH. Section III discusses the corresponding numerical methodology to build the disks. Sequences of equilibrium models are presented in Section IV along with the discussion of their morphological features and properties. Finally, our conclusions are summarized in Section V. Geometrized units ($G = c = 1$) are used throughout.

II. FRAMEWORK

A. Spacetime metric and KBHsSH models

The KBHsSH models we use in this study are built following the procedure described in [22]. The underlying theoretical framework is the Einstein-Klein-Gordon (EKG) field theory, describing a massive complex scalar field Ψ minimally coupled to Einstein gravity. KBHsSH solutions are obtained by using the following ansatz for the metric and the scalar field [2]

$$\begin{aligned} ds^2 &= e^{2F_1} \left(\frac{dr^2}{N} + r^2 d\theta^2 \right) + e^{2F_2} r^2 \sin^2 \theta (d\phi - W dt)^2 \\ &- e^{2F_0} N dt^2, \end{aligned} \quad (1)$$

$$\Psi = \phi(r, \theta) e^{i(m\varphi - \omega t)}, \quad (2)$$

with $N = 1 - r_H/r$, where r_H is the radius of the event horizon of the BH, and W, F_1, F_2, F_0 are functions of r and θ . Moreover, ω is the scalar field frequency and m is the azimuthal harmonic index.

The stationary and axisymmetric metric ansatz is a solution to the EKG field equations $R_{ab} - \frac{1}{2}Rg_{ab} = 8\pi(T_{SF})_{ab}$ with

$$\begin{aligned} (T_{SF})_{ab} &= \partial_a \Psi^* \partial_b \Psi + \partial_b \Psi^* \partial_a \Psi \\ &- g_{ab} \left(\frac{1}{2} g^{cd} (\partial_c \Psi^* \partial_d \Psi + \partial_d \Psi^* \partial_c \Psi) + \mu^2 \Psi^* \Psi \right) \end{aligned} \quad (3)$$

where μ is the mass of the scalar field and superscript (*) denotes complex conjugation. The interested reader is addressed to [22] for details on the equations of motion for the scalar field Ψ and the four metric functions W, F_0, F_1, F_2 , along with their solution.

Table I lists the seven KBHsSH models we use in this work. The models have been selected to span all regions of interest in the parameter space. Model I corresponds to a Kerr-like model, with almost all the mass and angular momentum stored in the BH, while model VII corresponds to a hairy Kerr BH with almost all the mass and angular momentum stored in the scalar field. It is worth mentioning that some of the models violate the Kerr bound (i.e. the normalized spin parameter is larger than 1) in terms of both ADM or horizon quantities.

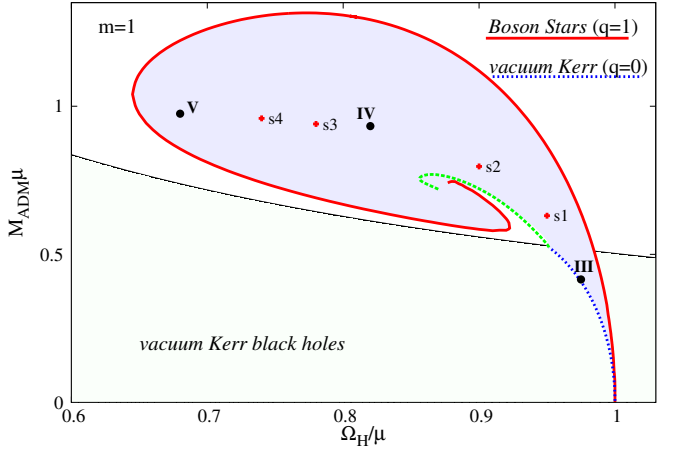


FIG. 1. Domain of existence for KBHsSH in an ADM mass versus scalar field frequency diagram. **TF:** The figure has to be redone to label the 7 models used in this work.

This is not a source of concern because, as shown in [23], the linear velocity of the horizon, v_H , never exceeds 1. For comparison, we also show in the last column of Table I the spin parameter a_{Heq} corresponding to a Kerr BH with a horizon linear velocity v_H . **TF:** Further description of the table. Something must be said about the coordinates.. In addition to the information provided in Table I, Figure 1 plots the location of our models in the domain of existence of KBHsSH in an ADM mass versus scalar field frequency diagram. **TF:** This figure has to be redone.

B. Distribution of angular momentum in the disk

Equilibrium models of thick disks around Kerr BHs are built assuming that the spacetime metric and the fluid fields are stationary and axisymmetric (see, e.g. [21, 24, 25] and references therein). For disks around KBHsSH we can follow the same approach as the metric ansatz given by Eq. (1) is stationary and axisymmetric.

We start by introducing the specific angular momentum l and the angular velocity Ω employing the standard definitions,

$$l = -\frac{u_\phi}{u_t}, \quad \Omega = \frac{u^\phi}{u^t}, \quad (4)$$

where u^μ is the fluid four-velocity. The relationship between l and Ω is given by the equations

$$l = -\frac{\Omega g_{\phi\phi} + g_{t\phi}}{\Omega g_{t\phi} + g_{tt}}, \quad \Omega = -\frac{l g_{tt} + g_{t\phi}}{l g_{t\phi} + g_{\phi\phi}}, \quad (5)$$

where we are assuming circular motion, i.e. the four-velocity can be written as

$$u^\mu = (u^t, 0, 0, u^\phi). \quad (6)$$

TABLE I. List of models of KBHsSH used in this work. From left to right the columns report the name of the model, the ADM mass, M_{ADM} , the ADM angular momentum, J_{ADM} , the horizon mass, M_{H} , the horizon angular momentum, J_{H} , the mass of the scalar field, M_{SF} , the angular momentum of the scalar field, J_{SF} , the radius of the event horizon, r_{H} , the values of the normalized spin parameter for the ADM quantities, a_{ADM} , and for the BH horizon quantities, a_{H} , the horizon linear velocity, v_{H} , and the spin parameter corresponding to a Kerr BH with a linear velocity equal to v_{H} , $a_{\text{H}_{\text{eq}}}$.

Model	M_{ADM}	J_{ADM}	M_{H}	J_{H}	M_{SF}	J_{SF}	r_{H}	a_{ADM}	a_{H}	v_{H}	$a_{\text{H}_{\text{eq}}}$
I	0.415	0.172	0.393	0.150	0.022	0.022	0.200	0.9987	0.971	0.7685	0.9663
II	0.630	0.403	0.340	0.121	0.290	0.282	0.221	1.0140	0.376	0.6802	0.9301
III	0.797	0.573	0.365	0.172	0.432	0.401	0.111	0.9032	1.295	0.7524	0.9608
IV	0.933	0.739	0.234	0.114	0.699	0.625	0.100	0.8489	2.082	0.5635	0.8554
V	0.940	0.757	0.159	0.076	0.781	0.680	0.091	0.8560	3.017	0.4438	0.7415
VI	0.959	0.795	0.087	0.034	0.781	0.747	0.088	0.9477	3.947	0.2988	0.5487
VII	0.975	0.850	0.018	0.002	0.957	0.848	0.040	0.8941	6.173	0.0973	0.1928

The approach we followed in [21] for the angular momentum distribution of the disks was introduced by [20], and it is characterized by three free parameters, β , γ , and η (see Eq. (7) in [21]). In this work, for simplicity and to reduce the ample space of parameters, we consider a constant angular momentum distribution, $l(r, \theta) = \text{const}$, which corresponds to setting $\beta = \gamma = 0$ in [21]. This choice also allows for the presence of a cusp (and hence matter accretion onto the black hole) and a centre. **TF:** We should explain/motivate why we change our approach in this paper.**SG:** We limit this study to the constant angular momentum case to limit the parameter space, as the main aim of this paper is to study the dependence of the characteristics of magnetised discs with respect to the KBHSH spacetime. Following [25], the specific value of the angular momentum corresponding to bound fluid elements ($-u_t < 1$) is computed as the minimum of the following equation

$$l_b^\pm(r, \theta) = \frac{g_{t\phi} \pm \sqrt{(g_{t\phi}^2 - g_{tt}g_{\phi\phi})(1 + g_{tt})}}{-g_{tt}} \quad (7)$$

where the plus sign corresponds to prograde orbits and the minus sign to retrograde orbits. Our convention is that the angular momentum of the BH is positive and the matter of the disk rotates in the positive (negative) direction of ϕ for a prograde (retrograde) disk. Equation (7) is given by [25] for Kerr BHs, but it is valid for any stationary and axisymmetric spacetime. For prograde motion, the function has a minimum outside the event horizon. The location of this minimum corresponds with the marginally bound orbit r_{mb} , and the angular momentum corresponds to the Keplerian angular momentum l_{mb} at that point. We show the proof of this statement in Appendix A. **TF:** Is there an Appendix A?**SG:** Yes. Please, read Appendix A.

C. Magnetized disks

To account for the magnetic field in the disks we use the procedure described by [19, 26]. First, we write the

equations of ideal general relativistic MHD as the following conservation laws, $\nabla_\mu T^{\mu\nu} = 0$, $\nabla_\mu {}^*F^{\mu\nu} = 0$, and $\nabla_\mu(\rho u^\mu) = 0$, where ∇_μ is the covariant derivative and

$$T^{\mu\nu} = (\rho h + b^2)u^\mu u^\nu + (p + p_m)g^{\mu\nu} - b^\mu b^\nu, \quad (8)$$

is the energy-momentum tensor of a magnetized perfect fluid, h , ρ , p , and p_m being the fluid specific enthalpy, density, fluid pressure, and magnetic pressure, respectively, the latter defined as $p_m = b^2/2$. The ratio of fluid pressure to magnetic pressure defines the magnetization parameter $\beta_m = p/p_m$. Moreover, ${}^*F^{\mu\nu} = b^\mu u^\nu - b^\nu u^\mu$ is the (dual of the) Faraday tensor relative to an observer with four-velocity u^μ , and b^μ is the magnetic field in that frame, with $b^2 = b^\mu b_\mu$ (see [27] for further details). Assuming the magnetic field is purely azimuthal, i.e. $b^r = b^\theta = 0$, and taking into account that the flow is stationary and axisymmetric, the conservation of the current density and of the Faraday tensor follow. Contracting the divergence of Eq. (8) with the projection tensor $h^\alpha_\beta = \delta^\alpha_\beta + u^\alpha u_\beta$, we arrive at

$$(\rho h + b^2)u_\nu \partial_i u^\nu + \partial_i \left(p + \frac{b^2}{2} \right) - b_\nu \partial_i b^\nu = 0, \quad (9)$$

where $i = r, \theta$. This equation can be rewritten in terms of the specific angular momentum l and of the angular velocity Ω ,

$$\partial_i(|\ln u_t|) - \frac{\Omega \partial_i l}{1 - l\Omega} + \frac{\partial_i p}{\rho h} + \frac{\partial_i(\mathcal{L}b^2)}{2\mathcal{L}\rho h} = 0, \quad (10)$$

where $\mathcal{L} = g_{t\phi}^2 - g_{tt}g_{\phi\phi}$.

To integrate Eq. (10) we need to assume an equation of state (EOS). We assume a polytropic EOS of the form

$$p = K\rho^\Gamma, \quad (11)$$

with K and Γ constants. By introducing the definitions $\tilde{p}_m = \mathcal{L}p_m$, $w = \rho h$ and $\tilde{w} = \mathcal{L}(w)$, we can write equations equivalent to Eq. (11) for both \tilde{p}_m and p_m

$$\tilde{p}_m = M\tilde{w}^q, \quad (12)$$

$$p_m = M\mathcal{L}^{q-1}(\rho h)^q, \quad (13)$$

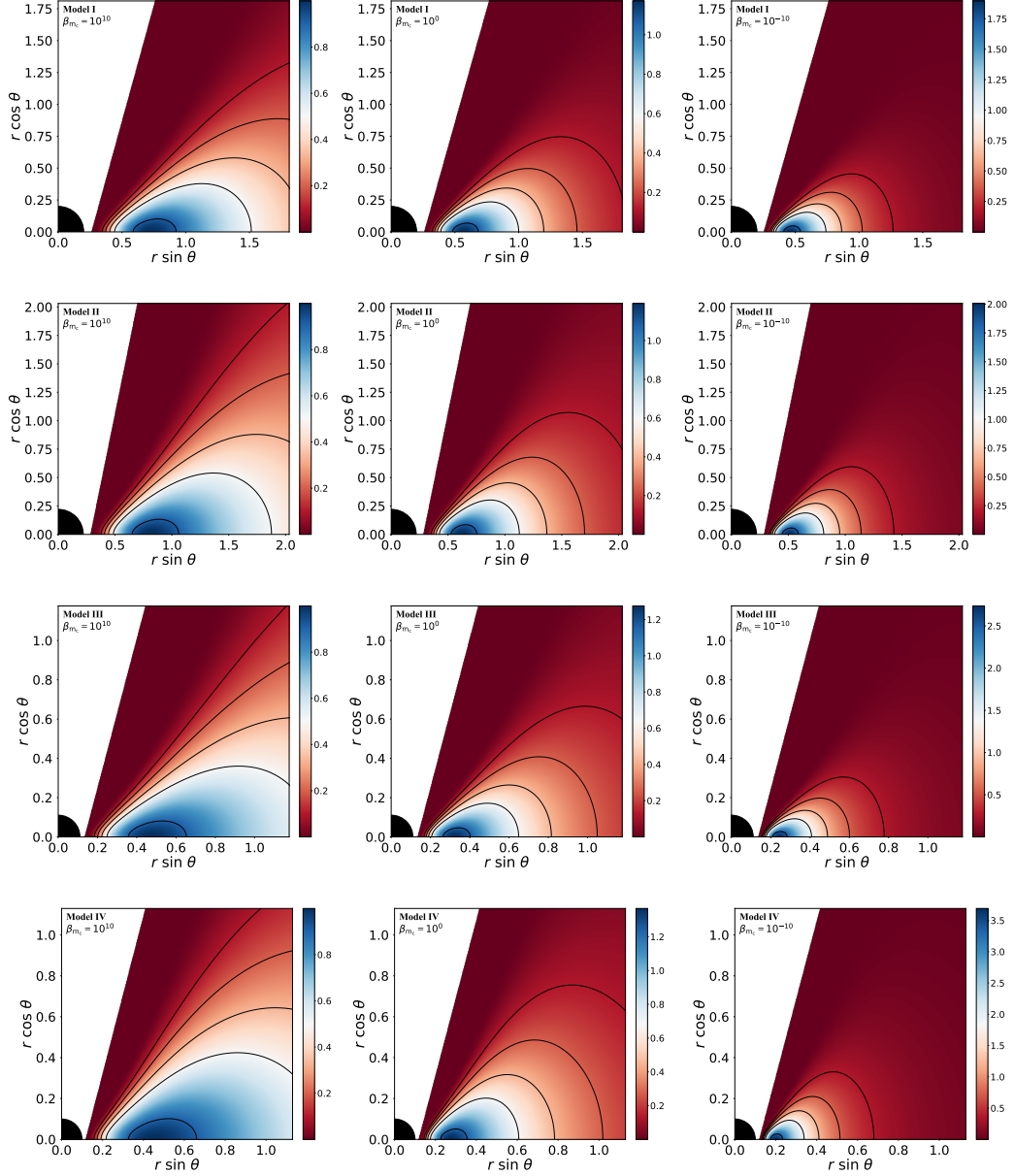


FIG. 2. Distribution of the rest-mass density. From top to bottom the rows correspond to the first four models of KBHsSH (I, II, III and IV). From left to right the columns correspond to different values of the magnetization parameter, namely non-magnetized ($\beta_{m_c} = 10^{10}$), mildly magnetized ($\beta_{m_c} = 1$) and strongly magnetized ($\beta_{m_c} = 10^{-10}$). The range of the colour scale is not the same for all plots. **TF:** Perhaps it would be good to include in the upper left corner of each plot a legend indicating the model (e.g. Model I) and the value of β_{m_c} . **SG:** Done.

where M and q are constants. Then we can integrate Eq. (10) as

$$W - W_{\text{in}} + \ln \left(1 + \frac{\Gamma K}{\Gamma + 1} \rho^{\Gamma-1} \right) + \frac{q}{q-1} M (\mathcal{L} \rho h)^{q-1} = 0, \quad (14)$$

where $W \equiv \ln |u_t|$ stands for the (gravitational plus centrifugal) potential and W_{in} is the potential at the inner edge of the disk.

We can also define the total energy density for the

torus, $\rho_T = -T_t^t + T_i^i$, and for the scalar field, $\rho_{\text{SF}} = -(T_{\text{SF}})_t^t + (T_{\text{SF}})_i^i$. These are given by

$$\rho_T = \frac{\rho h(g_{\phi\phi} - g_{tt}l^2)}{g_{\phi\phi} + 2g_{t\phi}l + g_{tt}l^2} + 2(p + p_m), \quad (15)$$

$$\rho_{\text{SF}} = 2 \left(\frac{2e^{-2F_0}w(w - mW)}{N} - \mu^2 \right) \phi^2. \quad (16)$$

Using these expressions, we can compute the total gravitational mass of the torus and the scalar field as the

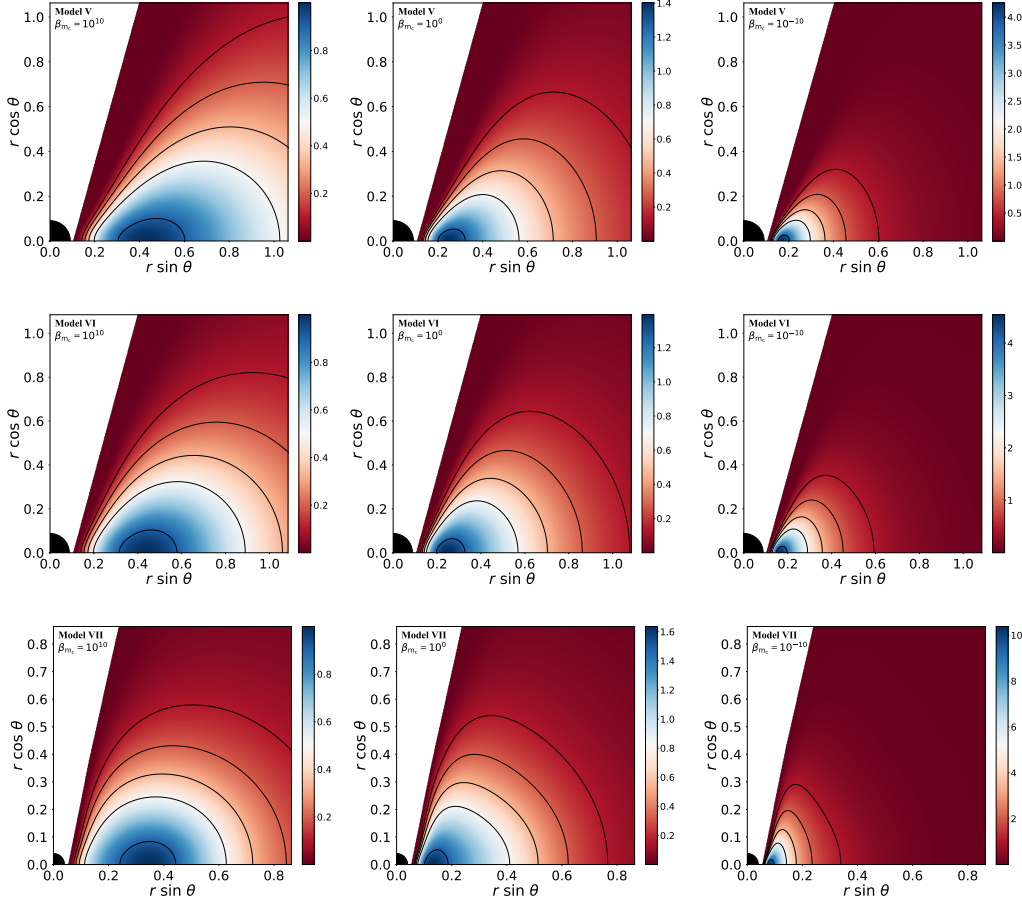


FIG. 3. Same as Fig. 2 but for the last three models of KBHsSH (V, VI, and VII). **TF:** Same comment as in the previous figure. **SG:** Done.

following expression

$$\mathcal{M} = \int \rho \sqrt{-g} d^3x \quad (17)$$

where g is the determinant of the metric tensor.

TF: We also have to emphasize somewhere in the paper that we do not fix $h = 1$. This is an important difference with respect to the work of [17]. **SG:** As a concluding remark, it is worth to note that we are taking a different approach to construct the magnetised discs than the standard one [19] (this approach was also taken by [17] for discs around the same kind of KBHsSH we have in this work). As it is noted in [21], this approach considers implicitly assumes that the specific enthalpy is close to 1 ($w = ph \simeq \rho$). This means that the polytropic equation Eq. (11) can be written as $p = Kw^\Gamma$ (see Eq. (27) of [19]). To better understand the differences between this two approaches, we can consider their behaviour in two limiting cases, namely the non-magnetised case and the extremely magnetised case. For the non-magnetised case, we can rewrite Eq. (14) in the limiting case of $\beta_{m_e} \rightarrow \infty$

($M \rightarrow 0$) as

$$W - W_{\text{in}} + \ln \left(1 + \frac{\Gamma K}{\Gamma + 1} \rho^{\Gamma-1} \right) = 0. \quad (18)$$

Then, we can solve this equation for the specific enthalpy h

$$h = e^{W_{\text{in}} - W}. \quad (19)$$

Now, we want to obtain an analogous equation for the $h \simeq 1$ case. We start by considering Eq. (20) of [21] and taking the limit $\beta_{m_e} \rightarrow \infty$ (in this equation, this means $K_m \rightarrow 0$), to obtain

$$W - W_{\text{in}} + \frac{\Gamma K}{\Gamma + 1} w^{\Gamma-1}. \quad (20)$$

If we consider the $h \simeq 1$ approximimation, we can use the definition of h and solve the equation to arrive at

$$h = 1 + (W_{\text{in}} - W). \quad (21)$$

If we compare both results, we can see that Eq. (21) is the first order Taylor series expansion of Eq. (19) for a

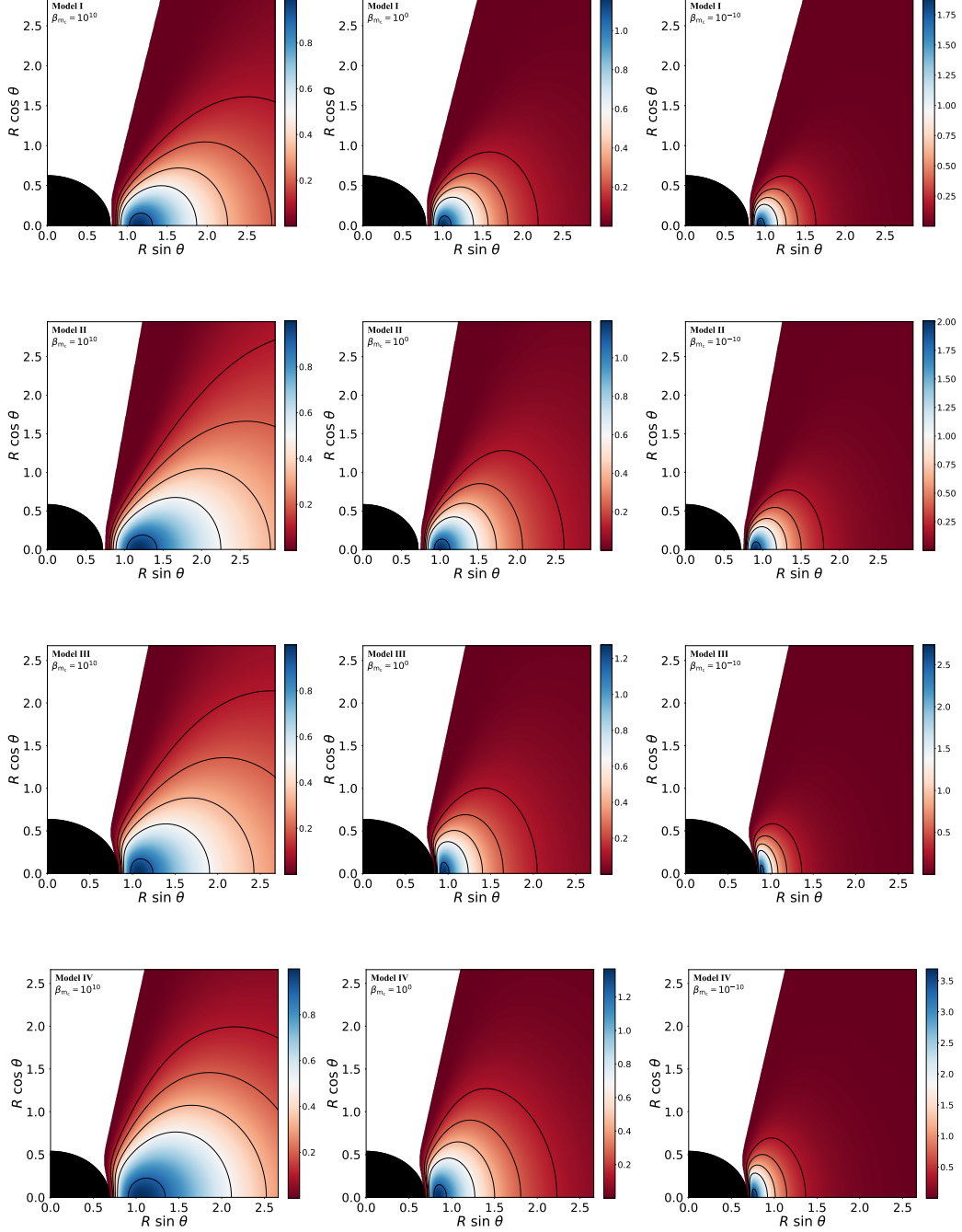


FIG. 4. Same as Fig. 2 but using the perimetral radial coordinate R . TF: Same comment as in the previous figure. SG: Done.

sufficiently small value of $W_{\text{in}} - W$. For the extremely magnetised case, we consider again Eq. (14) and Eq. (20) of [21], but this time we take $\beta_{m_c} \rightarrow 0$ ($K \rightarrow 0$). This yields the same result for both equations

$$W - W_{\text{in}} + \frac{q}{q-1} M(\mathcal{L}\rho h)^{q-1} = 0. \quad (22)$$

In addition, we could consider the expression for the spe-

cific enthalpy in terms of the density $h = 1 + \frac{K\Gamma\rho^{1-\Gamma}}{\Gamma-1}$ to see that we will have $h \rightarrow 1$. This shows that, for the extremely magnetised limit, this two approaches coincide. In conclusion, taking into account this two limits of both approaches we can discuss the range of validity of the $h \simeq 1$ approximation: As magnetised discs exist between the two considered cases, for discs with a sufficiently small value of the potential well $\Delta W \equiv W_{\text{in}} - W_c$,

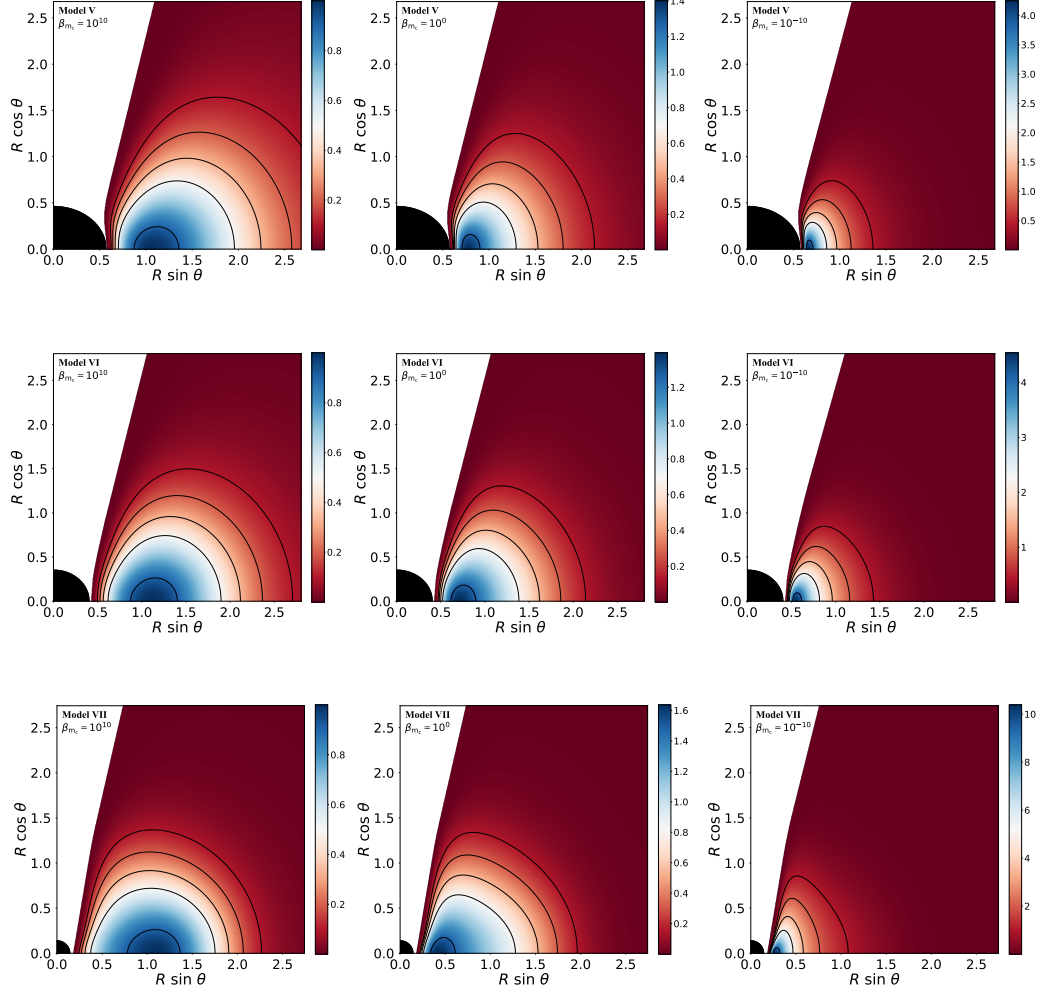


FIG. 5. Same as Fig. 3 but using the perimetral radial coordinate R . **TF:** Same comment as in the previous figure. **SG:** Done.

we can use the $h \simeq 1$ approximmaition without fear. On the other hand, if the value of ΔW is large enough, the approximmaition could fail even for fairly small magnetised discs.

III. METHODOLOGY

SG: This whole section is rewritten.

TF: Probably we do not need to have two subsections in this section, but just one. The description of the methodology is very poor now. It needs a lot of rewriting. **SG:** I have serious doubts about this section, as I am not really certain that we need to provide an explanation for some specific parts (that are pretty obvious anyway) Perhaps I should go into detail for the numerical part? (e.g. that Eq. (14) is a trascendental equation and we are bound to solve it numerically with the bisection method for each cell of our numerical grid)

From the previous discussion it becomes apparent that

the number of parameters defining the disk models is fairly large. In order to reduce the sample, in this work we set the mass of the scalar field $\mu = 1$, the exponents of the polytropic EOS to $q = \Gamma = 4/3$, the density at the centre of the disk $\rho_c = 1$, the specific angular momentum to $l = l_{mb}$ and the inner radius of the disk to $r_{in} = r_{mb}$. Thus, we leave the magnetization at the centre β_{mc} as the only free parameter for each model of KBHsSH. With this information we can compute all relevant physical quantities. **SG:** I have moved this paragraph from the above section to this one as I find it fits more naturally here. **TF:** We should discuss a bit more the reason for this choice. If $l_{ms} < l < l_{mb}$ and $r_{mb} < r_{cusp} < r_{ms}$ the disk is closed and has a centre and a cusp. If $l = l_{mb}$ and $r_{cusp} = r_{mb}$ the disk has a centre and a cusp, and it is closed at infinity. The models we have built are the latter, right? I wonder if we should have built models not completely filling their Roche lobe, so that they had a finite size. In any case, a comment must be provided here. **SG:** We choose this value for the angular momentum and

the inner radius of the disc to allow discs with a cusp and a centre that also are marginally stable (a small perturbation can trigger accretion into the black hole). Also, the thermodynamical quantities reach its maximum for this particular choice of angular momentum and inner radius of the disc (as they are related to the total potential well $|\Delta W|$). This also means that the resulting discs will be semi-infinite (they are closed at infinity), this is not a source of concern, as the external layers of the disc have extremely low density. (not sure about the relevance of the last part...) In particular, this choice of specific angular momentum distribution and inner radius of the disc is taken to allow discs with a cusp and a centre that also are marginally stable (a small perturbation can trigger accretion into the black hole). In addition, the thermodynamical quantities reach their maximum for this particular choice of parameters (as they are related to the total potential well $|\Delta W|$) SG: I am not sure if this needs further explanation.) This also means that the resulting discs will be semi-infinite (they are closed at infinity) but this is not a source of concern, as the external layers of the disc have extremely low density and, at some point, the value will be lower than the density of the atmosphere.

Before starting to build the disc, it is important to note that we need a sufficiently fine numerical grid in order to fully capture the behaviour of the physical magnitudes at the inner region of the disc. For that reason, we use a non-uniform grid (r, θ) with a domain $[r_H, 199.2] \times [0, \pi/2]$ and a number of points $N_r \times N_\theta = 2500 \times 300$. This means a radial resolution of $\simeq 0.001$ at the location of the disc centre. SG: This is a rough approximation, as this exact number depend on the horizon radius r_H and on the specific model. Nevertheless, the value of the resolution is much better at the cusp, specially if the disk is very close to the horizon (for instance in the $a = 0.9999$ Kerr case). Maybe we should clarify this, as these high spin cases need a very high radial resolution. Also, it may be important to note that it seems that we have not angular resolution enough to resolve the morphology of the disk in these extreme cases (see the 2D perimeteral plots). But I think this should go in the results section. SG: I am not sure if we have to tell something about the *real initial data* (i.e. the data provided by Carlos). Next, we first need to find l_{mb} and r_{mb} as the minimum of Eq. (7) and the location of said minimum in terms of the radial coordinate respectively. Once we have that, we can compute the total potential distribution as

$$W(r, \theta) \equiv \ln |u_t| = \frac{1}{2} \ln \left| \frac{g_{t\phi}^2 - g_{tt}g_{\phi\phi}}{g_{\phi\phi} + 2g_{t\phi}l + g_{tt}l^2} \right|. \quad (23)$$

With the total potential distribution, we can compute the location of the cusp r_{cusp} and the centre r_c as the extrema (maximum and minimum respectively) of the total potential in the equatorial plane. Also, we set $r_{in} = r_{cusp}$. For our choice of angular momentum distribution, this also means $W_{in} = 0$. Having now the total potential

distribution and the characteristic radii of the disc, we can start to compute the thermodynamical quantities in the disc. First of all, we compute the polytropic constant K evaluating Eq. (14) at the centre

$$W - W_{in} + \ln \left(1 + \frac{\Gamma K}{\Gamma + 1} \rho_c^{\Gamma-1} \right) + \frac{q}{q-1} \frac{K \rho_c^\Gamma}{\beta_{mc}(\rho_c + \frac{K \Gamma \rho_c^\Gamma}{\Gamma-1})} = 0 \quad (24)$$

where we have used the definition of magnetic pressure and the definition of the magnetisation parameter β . Using its corresponding definitions, we can also compute h_c , p_c , p_{mc} and the constant of the magnetic EOS M . With both K and M obtained, we can now compute the thermodynamical quantities in all our numerical domain. For points with $W(r, \theta) > 0$ we set $\rho = p = p_m = 0$ and for points with $W_c < W(r, \theta) < 0$, we write Eq. (14) as

$$W - W_{in} + \ln \left(1 + \frac{\Gamma K}{\Gamma + 1} \rho^{\Gamma-1} \right) + \frac{q}{q-1} M \left(\mathcal{L} \left(\rho + \frac{K \Gamma \rho^\Gamma}{\Gamma - 1} \right) \right)^{q-1} = 0, \quad (25)$$

to compute the rest-mass density ρ of said point. Then, we can use again Eqs. (11) and (12) and the definition of the specific enthalpy to compute the distribution of p , p_m and h .

It is relevant to note that Eqs. (24) and (25) are trascendental equations and that, particularly Eq. (25) must be solved at each point of our numerical grid. To solve these equations we use the bisection method. To ensure the accuracy of our computations (particularly the accuracy of the maximum and central quantities we report) we choose our grid to have a difference between two adjacent points of $\Delta r(r \simeq r_c) \simeq 0.001$ in the equatorial plane.

IV. RESULTS

A. 2D Morphology

We start presenting the morphological distribution of the models in the $(r \sin \theta, r \cos \theta)$ plane in figures 2 and 3. The radial coordinate in these figures is the standard one of the spherical coordinate system. Figures 2 and 3 show the rest-mass density distribution for all our KBHsSH models for 3 different values of the magnetization parameter at the centre of the disks, β_{mc} , namely 10^{10} (unmagnetized, left column), 1 (mildly magnetized, middle column) and 10^{-10} (strongly magnetized, right column).

The structure of the disks is similar for all values of β_{mc} with the only quantitative differences being the location of the centre of the disk, which moves closer to the BH as the magnetization increases, and the range of variation of the isodensity contours, whose upper ends become larger with decreasing β_{mc} . This behaviour is in complete agreement with that found for KBHs in [21] irrespective of the BH spin. For the particular case of Model VII, the maximum of the rest-mass density for the strongly magnetized case is significantly larger than

TABLE II. Values of the relevant physical magnitudes of our models of magnetized, equilibrium tori around KBHsSH. For all cases, $R_{\text{in}} = R_{\text{mb}}$ and $l = l_{\text{mb}}$. **TF:** Are we using the perimetral radial coordinate in this table? **SG:** Yes.

Model	l	W_c	R_{in}	R_c	β_{m_c}	h_{max}	ρ_{max}	p_{max}	$p_{m,\text{max}}$	R_{max}	$R_{m,\text{max}}$
I	0.934	−0.188	0.81	1.14	10^{10}	1.21	1.0	5.16×10^{-2}	5.50×10^{-12}	1.14	1.26
					1	1.10	1.17	3.11×10^{-2}	2.68×10^{-2}	1.01	1.06
					10^{-10}	1.0	1.90	1.10×10^{-11}	7.80×10^{-2}	0.93	0.96
II	0.933	−0.205	0.75	1.18	10^{10}	1.23	1.0	5.69×10^{-2}	6.14×10^{-12}	1.18	1.36
					1	1.12	1.19	3.50×10^{-2}	2.97×10^{-2}	1.00	1.07
					10^{-10}	1.0	2.01	1.30×10^{-11}	8.99×10^{-2}	0.91	0.94
III	1.060	−0.362	0.84	1.07	10^{10}	1.44	1.0	0.109	1.21×10^{-11}	1.07	1.22
					1	1.23	1.28	7.22×10^{-2}	5.76×10^{-2}	0.95	0.99
					10^{-10}	1.0	2.74	3.48×10^{-11}	0.206	0.89	0.91
IV	1.160	−0.547	0.67	1.06	10^{10}	1.723	1.0	0.182	2.09×10^{-11}	1.06	1.34
					1	1.38	1.37	0.129	9.76×10^{-2}	0.85	0.91
					10^{-10}	1.0	3.70	7.83×10^{-11}	0.408	0.76	0.78
V	1.200	−0.685	0.58	1.07	10^{10}	1.98	1.0	0.246	2.76×10^{-11}	1.07	1.31
					1	1.51	1.40	0.178	0.132	0.78	0.87
					10^{-10}	1.0	4.26	1.18×10^{-10}	0.579	0.67	0.69
VI	1.200	−0.832	0.43	1.12	10^{10}	2.30	1.0	0.324	3.52×10^{-11}	1.12	1.32
					1	1.66	1.39	0.228	0.169	0.72	0.86
					10^{-10}	1.0	4.54	1.57×10^{-10}	0.740	0.55	0.59
VII	0.920	−1.236	0.18	1.10	10^{-10}	3.44	1.0	0.610	6.459×10^{-11}	1.10	1.25
					1	2.25	1.64	0.510	0.322	0.43	0.62
					10^{-10}	1.0	10.42	7.03×10^{-10}	2.44	0.28	0.30

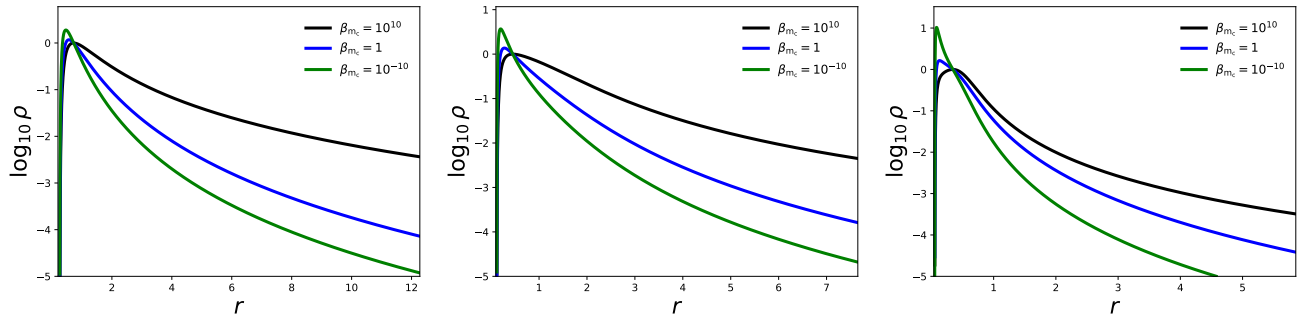


FIG. 6. Effects of the magnetization on the radial profiles of the logarithm of the density at the equatorial plane for different KBHsSH models. In each panel there are . Left panel: Model I. Central panel: Model IV. Right panel: Model VII.

for the other models and the spatial extent of the disk is significantly small. **TF:** Can we use the last isodensity contour as a good measure of the size of the disk? **SG:** In figure 6, we can visualise the radial extent for the models I, IV and VII with three different values of the magnetisation (10^{10} , 1, and 10^{-10}). As it can be seen, model I discs are significantly bigger than their model IV and VII counterparts. Also, it is important to note the presence of a thicker region of high density in the model VII non-magnetised case (the mildly-magnetised case also has it, but to a lesser extent). This could be related to the existence of an extra gravitational well that overlaps with the disc (as it can be seen in the right panel of figure 7).

In figures 4 and 5 we show the same models, but using a perimetral radial coordinate such as $R = e^{F_2} r$. **TF:** We need to justify why we introduce this new radial coordinate. What is the benefit? Please include an explanation and also describe briefly the differences/similarities between these two figures and the first two. **SG:** Discuss. I find that the 2D morphology in perimetral coordinates might not be very useful, but I found an interesting property of these coordinates: For the Kerr metric, $R_H = 2M$ irrespective of the value of the angular momentum (For the KBHsSH cases, $2M_H \neq R_H \neq 2M_{\text{ADM}}$. I don't know if there are any kind of dependence on the angular momentum, as we don't have two cases with the same value of

the mass). I suppose this could help us to compare different models. In fact, the differences in the morphology close to the equatorial plane in the near horizon region are actually related to the value of the angular momentum (we can see a relationship between the morphological differences and the equivalent spin parameter a_{eq}).

Table II reports the relevant physical quantities for our disk models around KBHsSH. First of all, it is worth to mention that KBHsSH can violate the Kerr bound for the potential $\Delta W \equiv W_{\text{in}} - W_c$. As shown in [28], constant angular momentum disks exhibit a maximum for $|\Delta W|$ when the spin parameter a approaches 1. This value is $\Delta W_{\text{max}} = -\frac{1}{2} \ln 3 \simeq -0.549$. The models V, VI and VII violate that bound. This is related, as we see, with the maximum value of the specific enthalpy, pressure and magnetic pressure. **SG:** The maximum value of these quantities increases with the total potential well ΔW , irrespective of the value of the magnetisation.

Table III reports the relevant physical quantities for the disks built around KBH. **SG:** As in the KBHsSH case, the maximum values of the enthalpy, density, pressure and magnetic pressure increase with increasing ΔW (in this case this also means increasing value of a). Also, it can be seen that both the cusp and the centre move closer to the horizon with increasing a . **TF:** Describe.

In figure 7 we show the total energy density of the torus ρ_T (upper half of each image) and the total energy density of the scalar field ρ_{SF} (lower half) for models I, IV and VII and 2 values of the magnetization parameter at the center (10^{10} , left panel, and 10^{-10} , right panel). **TF:** Describe this figure. **SG:** Not sure if we need to describe both figures separately. Maybe we only need one of them.

In figure 8, we show the same, but using the perimetal coordinate we defined earlier. The plots show that **SG:** , for the non-magnetised cases, the maximum of the total energy density of the disk ρ_T is closer to the maximum of the total energy density of the scalar field ρ_{SF} for increasing hair. **TF:** This trend is only satisfied for the unmagnetized models (top row) but not for the strongly magnetized models. **SG:** This trend disappears with increasing magnetisation, as the disc moves closer to the horizon.

TF: One question: in our approach we are building the disks using the stress-energy tensor of the fluid only. Is this correct? Shouldn't we consider the entire stress-energy tensor from the fluid and the scalar field? Is this a valid approximation because we are in the test-fluid regime? What did [17] do? **SG:** They do the same as us. As we are considering the scalar field part of the spacetime (there is no interaction between the scalar field and the matter other than gravity) and we are in the test-fluid approximmation I think this is correct.

B. Comparison with KBHs

Also, in figures 11 and 12 we show different KBH models with the same mass $M_{\text{BH}} = 1$ and different values for

the spin parameter(0, 0.5, 0.9, 0.9999).

SG: I am thinking about merging this section with the others.

SG: Compare the radial profiles. **SG:** Describe and compare the angular velocity at the centre.

C. Magnetization profiles

The dependence of the maximum specific enthalpy h_{max} and the maximum rest-mass density ρ_{max} with the magnetization parameter is shown in figures 9. The upper panels correspond to the KBHsSH models (I-VII) and the lower ones to a sequence of KBHs with increasing spin parameter. **TF:** Maybe there is an excessive number of cases for KBHs. Maybe it's enough to only include the four cases we have in Table III. We could always indicate in the main text the values that are reached for an extreme value of a with seven 9. This will also simplify the presentation of this figure, where I don't like very much having lines and dots. Here we can see that, for both cases, an increase in $|\Delta W|$ implies higher values for h_{max} (low magnetization) and also higher values for ρ_{max} (high magnetization). However, there are differences between the two cases. For the enthalpy, the values of h_{max} reached for the KBHsSH are much higher than those of the KBH case. This fact tells us that, while the $w = \rho h \simeq \rho$ approximation (see [19] and [21]) is valid for magnetized flows ($\beta_{m_c} \sim 1$) for reasonable values of the spin parameter ($a \sim 0.99$ or lower), that is not the case for KBHsSH. Also, for the rest-mass density we have a different behaviour: ρ_{max} for KBHsSH reach values only attainable by high spin parameter KBHs (between $a = 0.9$ and $a = 0.99999$ for the seven models we present here).

Figure 10 shows the variation of the quotient of the perimetal radius of the magnetic pressure maximum by the perimetal radius of the disk center $R_{m,\text{max}}/R_c$ with the decimal logarithm of the magnetization parameter at the disk center $\log_{10} \beta_{m_c}$ for the same KBHsSH and KBH cases as in figure 9. The inset shows a region around $\beta_{m_c} = 3$ and $R_{m,\text{max}}/R_c = 1$, this is because for disks with $h = 1$, $R_{m,\text{max}} = R_c$ if $\beta_{m_c} = 1/\Gamma - 1$. As we can easily see, this condition is also fulfilled for the Kerr case, even $h \neq 1$ (with a slight deviation for very high spin parameter cases), but not quite for the KBHsSH cases. **SG:** At this point, it is relevant to remember that some of the KBHsSH models violate the Kerr bound in terms of the potential. As we mentioned previously, we need a small value of ΔW for the $h \simeq 1$ approximmation to be valid in the non-magnetised regime. Now we can see that, in the KBHsSH case, this approximmation is not valid even for mildly-magnetised discs.

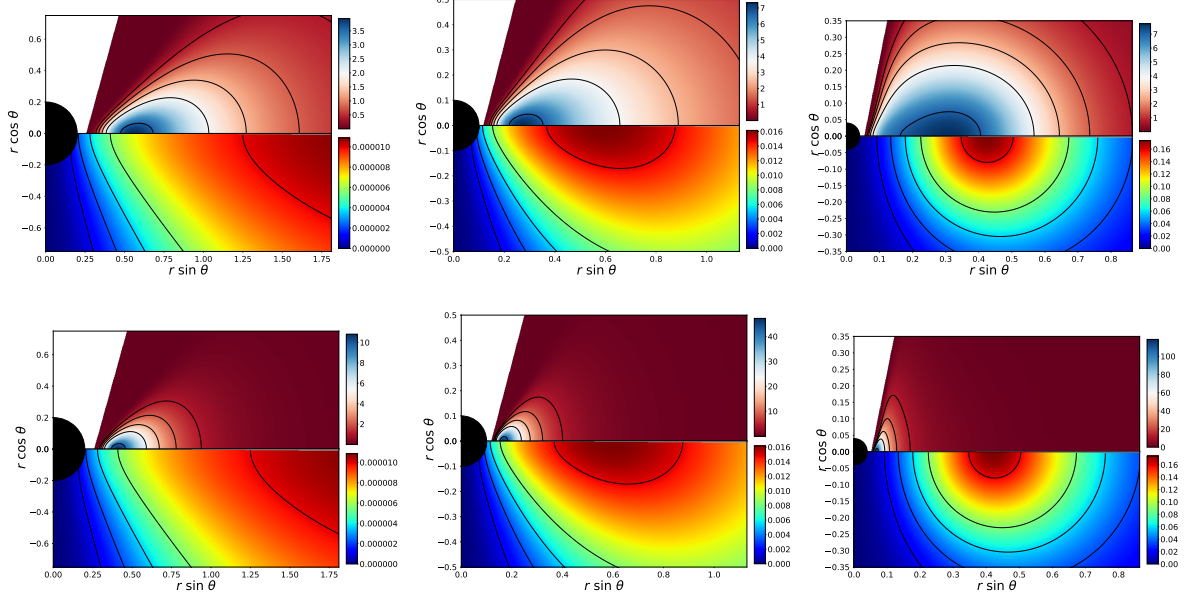


FIG. 7. Energy density distribution for the torus ρ_T (upper half of the images) and for the scalar field ρ_{SF} (lower half). From left to right the columns correspond to models I, IV, and VII. The top row corresponds to non-magnetized models ($\beta_{mc} = 10^{10}$) and the bottom row to strongly magnetized models ($\beta_{mc} = 10^{-10}$). TF: I think there is a lot of vertical space that we do not really need in these plots. To save some space, as we have many figures, I suggest to plot the vertical axis in shorter ranges, say $[-0.75, 0.75]$ for model I, $[-0.5, 0.5]$ for model IV, and $[-0.35, 0.35]$ for model VII (and keeping the horizontal axis as it is now). I know the plot will not look squared, but that's fine. SG: Done.

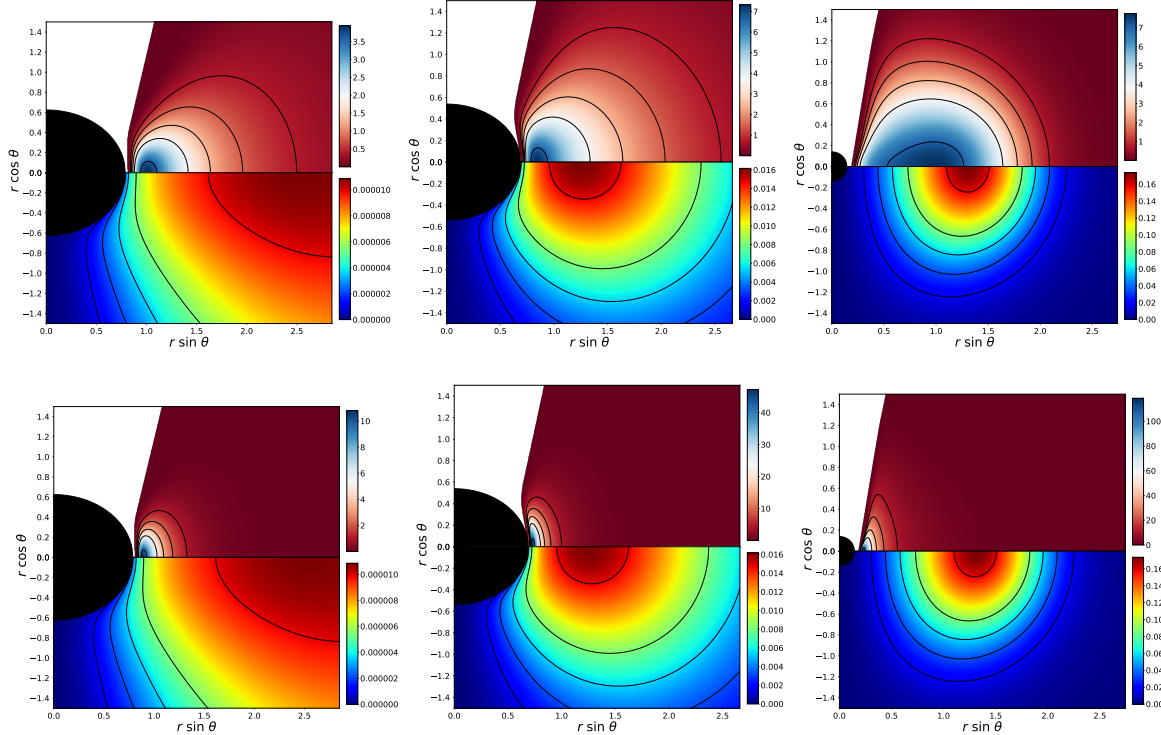


FIG. 8. Same as Fig. 7 but using the perimetral radial coordinate. TF: Same comment as in the previous figure regarding the vertical range, in this case $[-1.5, 1.5]$ for all models. SG: Done

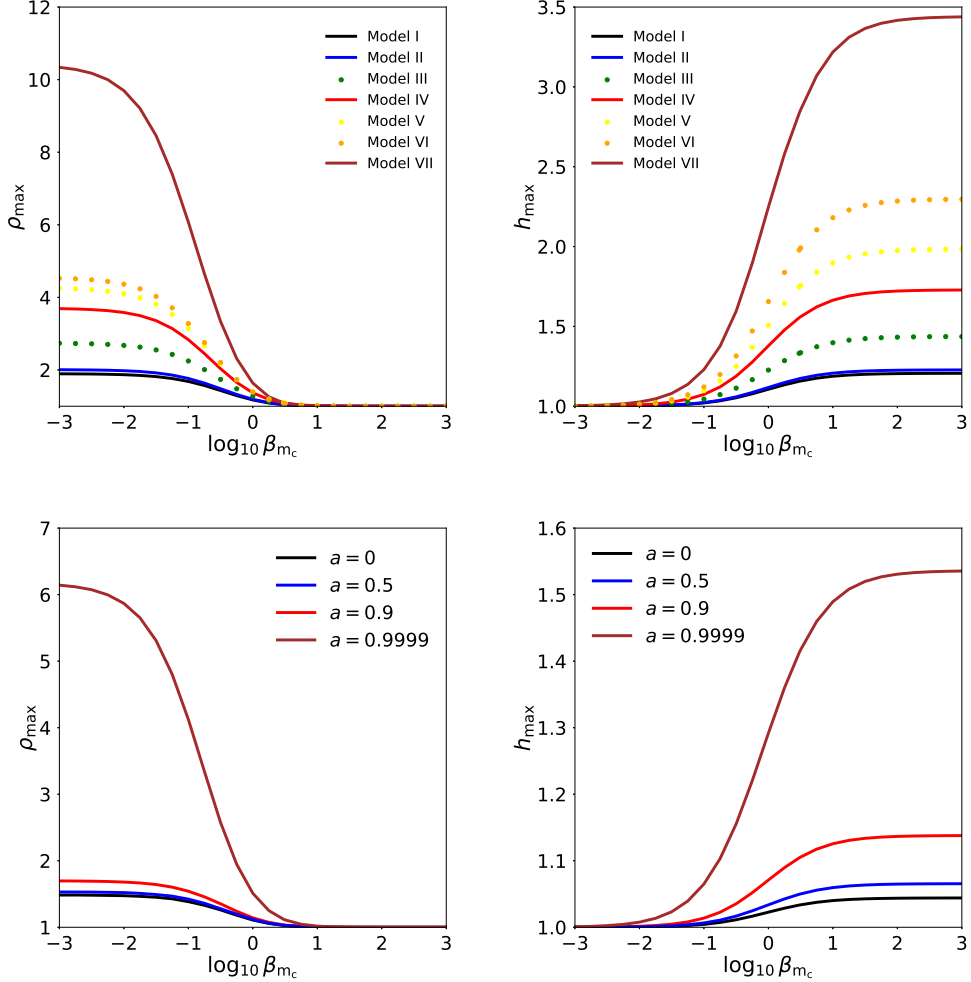


FIG. 9. Effects of the magnetization on the values for the maximum density (left) and enthalpy (right) of the disc. In the first row, we show this for all of our KBHsSH models. In the second row, we show this for a sequence of KBHs with increasing spin parameter.

D. Torus mass

SG: Even the models we have computed are non-self gravitating, for the sake of astrophysical relevance, we computed the mass of some of the discs. For this case only, we have dropped the $\rho_c = 1$ choice and instead, we have chosen that the mass of the torus must be $M_T = 0.1M_{\text{ADM}}$. This is in agreement with the torus masses found as the final state of binary neutron stars mergers

SG: I think here we should go further and do the following: First, choose a suitable maximum ADM mass for the KBHsSH (Eq (I.1) of [3]), this implies a choice of scalar field mass μ . This maximum mass should be such as our models ADM mass would be $\sim 2.5M_{\odot}$. Next, we should compute the central density for the models we want to compare (models I, IV, VII for 3 magnetisations and their Kerr ADM equivalents). Finally, we compute

the cgs central densities with the formula (From the book of Rezzolla *Relativistic Hydrodynamics*)

$$\rho_{\text{cgs}} = 6.17714 \times 10^{17} \left(\frac{G}{c^2} \right) \left(\frac{M_{\odot}}{M} \right)^2 \rho_{\text{geo}} \quad (26)$$

SG: and compare the central densities (or maximum) with known values.

V. CONCLUSIONS

Future work: Non-constant angular momentum case, Proca hair, shadows of the system HBH+disk.

ACKNOWLEDGMENTS

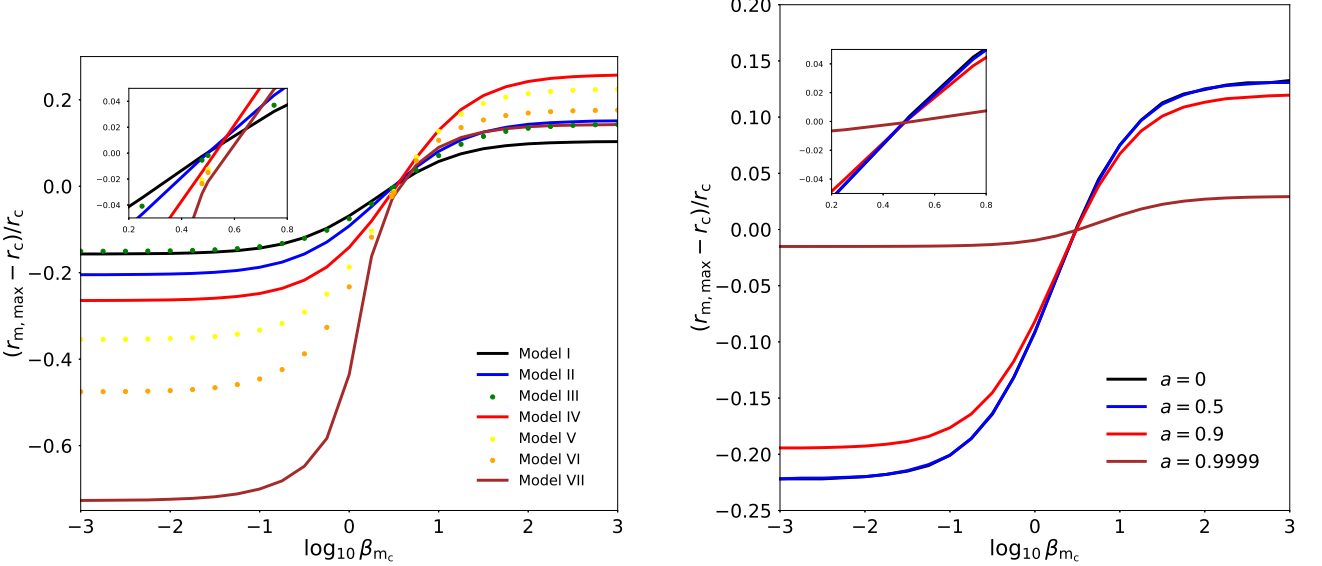


FIG. 10. Effects of the magnetization on the (perimeteral) location of the magnetic pressure maximum (divided by the the perimeteral radius of the centre) $((R_{\text{mag},\max} - R_c)/R_c)$. Left panel: KBHsSH models. Right panel: A sequence of KBHs with increasing spin parameter.

TABLE III. Disc parameters and values of their relevant physical magnitudes for the KBH case. For all the cases, we have $R_{\text{in}} = R_{\text{mb}}$, $l = l_{\text{mb}}$ and $M_{\text{BH}} = 1$.

a	l	W_c	R_{in}	R_c	β_{m_c}	h_{\max}	ρ_{\max}	p_{\max}	$p_{m,\max}$	R_{\max}	$R_{m,\max}$
0	4.00	-4.32×10^{-2}	4.00	10.47	10^{10}	1.04	1.0	1.10×10^{-2}	1.15×10^{-12}	10.47	11.86
					1	1.02	1.11	6.29×10^{-3}	5.69×10^{-3}	8.81	9.52
					10^{-10}	1.0	1.48	1.83×10^{-12}	1.48×10^{-2}	7.70	8.14
0.5	3.41	-6.35×10^{-2}	2.99	7.12	10^{10}	1.07	1.0	1.64×10^{-2}	1.72×10^{-12}	7.19	8.14
					1	1.03	1.12	9.43×10^{-3}	8.47×10^{-3}	6.05	6.53
					10^{-10}	1.0	1.53	2.81×10^{-12}	2.23×10^{-2}	5.29	5.59
0.9	2.63	-0.129	2.18	3.78	10^{10}	1.14	1.0	1.64×10^{-2}	3.65×10^{-12}	3.78	4.23
					1	1.07	1.14	2.03×10^{-2}	1.78×10^{-2}	3.25	3.47
					10^{-10}	1.0	1.70	6.54×10^{-12}	4.92×10^{-2}	2.92	3.04
0.9999	2.02	-0.429	2.00015	2.034	10^{10}	1.54	1.0	0.134	1.61×10^{-11}	2.034	2.094
					1	1.29	1.51	0.110	7.52×10^{-2}	2.0075	2.014
					10^{-10}	1.0	6.17	1.22×10^{-10}	0.491	2.0021	2.0030

- [1] C. A. R. Herdeiro and E. Radu, International Journal of Modern Physics D **24**, 1542014-219 (2015), arXiv:1504.08209 [gr-qc].
- [2] C. A. R. Herdeiro and E. Radu, Physical Review Letters **112**, 221101 (2014), arXiv:1403.2757 [gr-qc].
- [3] C. Herdeiro, E. Radu, and H. Rúnarsson, Classical and Quantum Gravity **33**, 154001 (2016), arXiv:1603.02687 [gr-qc].
- [4] W. E. East and F. Pretorius, Physical Review Letters **119**, 041101 (2017), arXiv:1704.04791 [gr-qc].
- [5] C. A. R. Herdeiro and E. Radu, Physical Review Letters **119**, 261101 (2017).
- [6] N. Sanchis-Gual, J. C. Degollado, P. J. Montero, J. A. Font, and C. Herdeiro, Physical Review Letters **116**, 141101 (2016), arXiv:1512.05358 [gr-qc].
- [7] P. Bosch, S. R. Green, and L. Lehner, Physical Review Letters **116**, 141102 (2016), arXiv:1601.01384 [gr-qc].
- [8] B. Ganchev and J. E. Santos, Physical Review Letters **120**, 171101 (2018), arXiv:1711.08464 [gr-qc].
- [9] J. C. Degollado, C. A. R. Herdeiro, and E. Radu, Physics Letters B **781**, 651 (2018), arXiv:1802.07266 [gr-qc].
- [10] B. P. Abbott, R. Abbott, T. D. Abbott, M. R. Abernathy, F. Acernese, K. Ackley, C. Adams, T. Adams, P. Addesso, R. X. Adhikari, and et al., Physical Review Letters **116**, 061102 (2016), arXiv:1602.03837 [gr-qc].

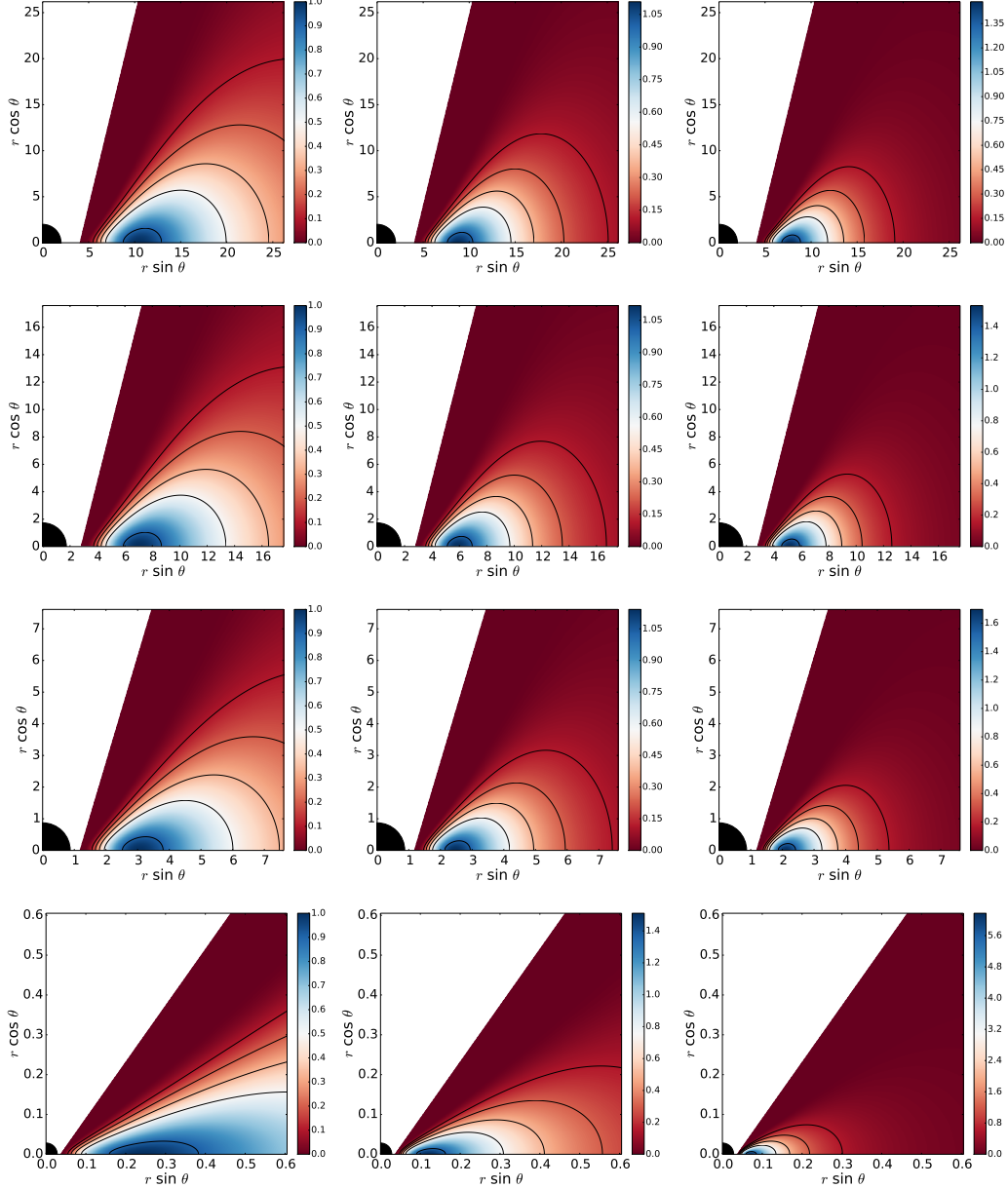


FIG. 11. Rest-mass density distribution. From top to bottom the rows correspond to a sequence of KBHs with increasing spin parameter a (0, 0.5, 0.9 and 0.9999). From left to right the columns correspond to different values of the magnetization parameter, namely non-magnetized ($\beta_{m_c} = 10^{10}$), mildly magnetized ($\beta_{m_c} = 1$) and strongly magnetized ($\beta_{m_c} = 10^{-10}$)

- [11] B. P. Abbott *et al.* (Virgo, LIGO Scientific), Phys. Rev. Lett. **116**, 241103 (2016), arXiv:1606.04855 [gr-qc].
- [12] B. P. Abbott *et al.* (VIRGO, LIGO Scientific), Phys. Rev. Lett. **118**, 221101 (2017), arXiv:1706.01812 [gr-qc].
- [13] B. P. Abbott *et al.* (Virgo, LIGO Scientific), Phys. Rev. Lett. **119**, 141101 (2017), arXiv:1709.09660 [gr-qc].
- [14] B. P. Abbott *et al.* (Virgo, LIGO Scientific), Astrophys. J. **851**, L35 (2017), arXiv:1711.05578 [astro-ph.HE].
- [15] V. Fish, K. Akiyama, K. Bouman, A. Chael, M. Johnson, S. Doeleman, L. Blackburn, J. Wardle, and W. Freeman, Galaxies **4**, 54 (2016), arXiv:1607.03034 [astro-ph.IM].
- [16] P. V. P. Cunha, C. A. R. Herdeiro, E. Radu, and H. F. Rúnarsson, Physical Review Letters **115**, 211102 (2015), arXiv:1509.00021 [gr-qc].
- [17] F. H. Vincent, E. Gourgoulhon, C. Herdeiro, and E. Radu, Phys. Rev. D **94**, 084045 (2016), arXiv:1606.04246 [gr-qc].
- [18] M. A. Abramowicz and P. C. Fragile, Living Reviews in Relativity **16**, 1 (2013), arXiv:1104.5499 [astro-ph.HE].
- [19] S. S. Komissarov, MNRAS **368**, 993 (2006), astro-ph/0601678.
- [20] L. Qian, M. A. Abramowicz, P. C. Fragile, J. Horák, M. Machida, and O. Straub, A&A **498**, 471 (2009), arXiv:0812.2467.
- [21] S. Gimeno-Soler and J. A. Font, Astron. Astrophys. **607**, A68 (2017), arXiv:1707.03867 [gr-qc].

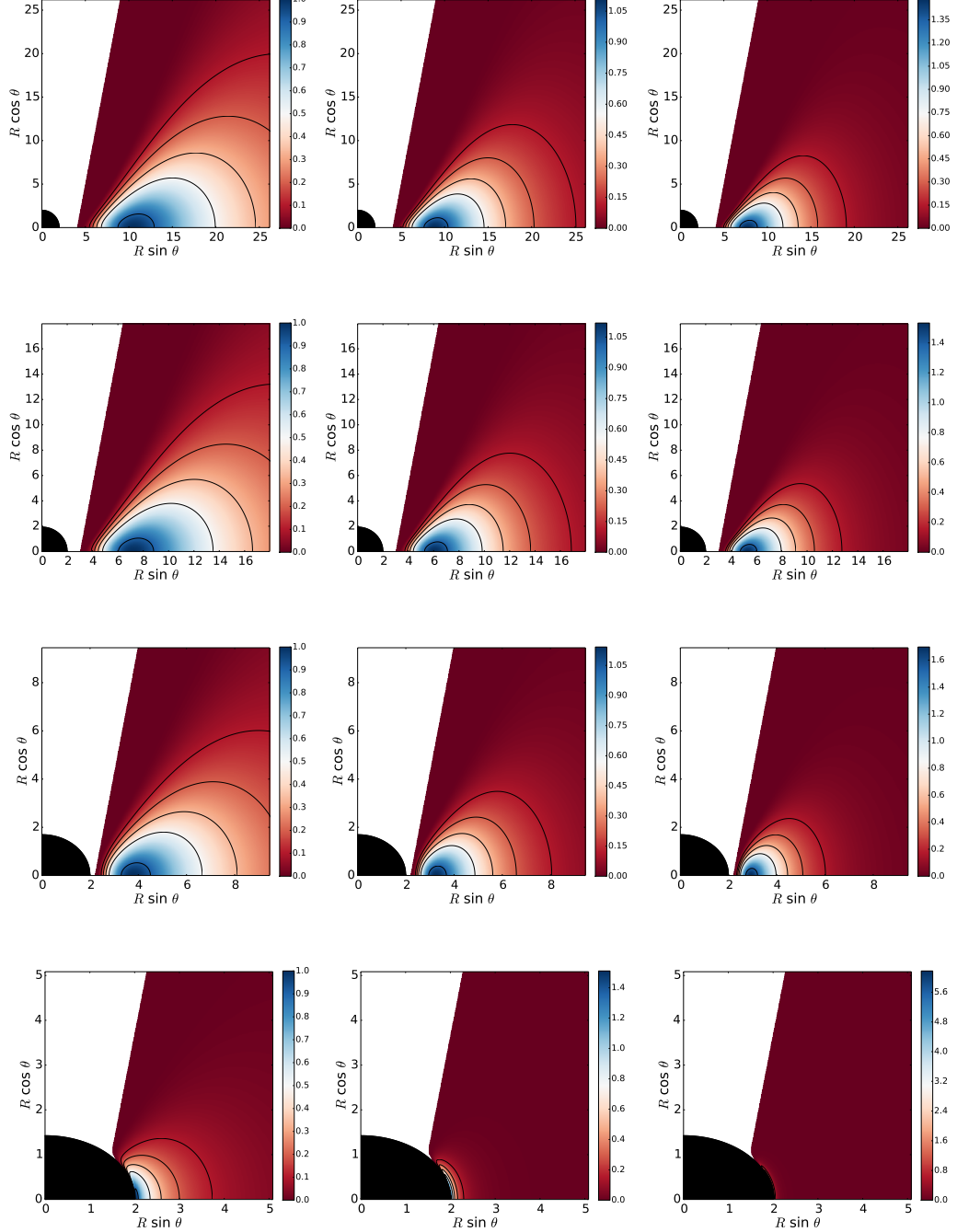


FIG. 12. Rest-mass density distribution using perimetric coordinates. From top to bottom the rows correspond to a sequence of KBHs with increasing spin parameter a (0, 0.5, 0.9 and 0.9999). From left to right the columns correspond to different values of the magnetization parameter, namely non-magnetized ($\beta_{mc} = 10^{10}$), mildly magnetized ($\beta_{mc} = 1$) and strongly magnetized ($\beta_{mc} = 10^{-10}$)

- [22] C. Herdeiro and E. Radu, Classical and Quantum Gravity **32**, 144001 (2015), arXiv:1501.04319 [gr-qc].
- [23] C. A. R. Herdeiro and E. Radu, International Journal of Modern Physics D **24**, 1544022 (2015), arXiv:1505.04189 [gr-qc].
- [24] J. A. Font and F. Daigne, MNRAS **334**, 383 (2002), astro-ph/0203403.
- [25] F. Daigne and J. A. Font, MNRAS **349**, 841 (2004), astro-ph/0311618.
- [26] P. J. Montero, O. Zanotti, J. A. Font, and L. Rezzolla, MNRAS **378**, 1101 (2007), astro-ph/0702485.

TABLE IV. Angular velocity at the centre for the different models computed. In the first column, we present the angular velocity at the disc centre for the different KBHsSH models. In the second column, we present the angular velocity at the disc centre for a KBH with the same ADM quantities. **SG: to fill with the Kerr case values.**

Model	Ω_c	Ω_{ADM_c}
I	0.493	—
II	0.424	—
III	0.521	—
IV	0.427	—
V	0.394	—
VI	0.350	—
VII	0.330	—

TABLE V. Central density of the disc for the different models, considering a disc with a value of r_{in} such as $\Delta W = 0.9\Delta W_{\text{Total} \equiv W_{\text{cusp}} - W_c}$ and a torus gravitational mass of $M_T = 0.1M_{\text{ADM}}$. In the first column, we present the value of the central density for the different KBHsSH models. In the second column, we present the central density for a KBH with the same ADM quantities. **SG: To fill with the Kerr case values.**

Model	β_{m_c}	ρ_c	ρ_{ADM_c}
I	10^{10}	0.002051	—
	1	0.00434	—
II	10^{-10}	0.00531	—
	10^{10}	0.00150	—
III	10^{-10}	0.00427	—
	10^{10}	0.00582	—
IV	10^{10}	0.00304	—
	1	0.00840	—
V	10^{-10}	0.0108	—
	10^{10}	0.00407	—
VI	10^{-10}	0.00897	—
	10^{10}	0.0110	—
VII	10^{10}	0.00577	—
	1	0.0104	—
VII	10^{-10}	0.0121	—
	10^{10}	0.00762	—
VII	1	0.0116	—
	10^{-10}	0.0131	—
VII	10^{10}	0.0129	—
	1	0.0162	—
VII	10^{-10}	0.01701	—

- [27] L. Antón, O. Zanotti, J. A. Miralles, J. M. Martí, J. M. Ibáñez, J. A. Font, and J. A. Pons, ApJ **637**, 296 (2006), astro-ph/0506063.
- [28] M. Abramowicz, M. Jaroszynski, and M. Sikora, A&A **63**, 221 (1978).

Appendix A: Finding l_{mb} and r_{mb}

SG: I figured this out, but now I am not really sure if this is interesting enough to be an appendix by itself. Maybe more like a comment in the main text. We start by considering the lagrangian of a stationary and axisymmetric spacetime

$$L = \frac{1}{2} \left(g_{tt}(\dot{t})^2 + 2g_{t\phi}\dot{t}\dot{\phi} + g_{rr}(\dot{r})^2 + g_{\theta\theta}(\dot{\theta})^2 + g_{\phi\phi}(\dot{\phi})^2 \right) \quad (\text{A1})$$

where $x^\alpha = dx^\alpha/d\lambda$ denotes the partial derivative of the coordinates with respect to an affine parameter λ . We can note that we have two cyclic coordinates (t and ϕ). Then, the canonically conjugate momentum of each coordinate is conserved, namely

$$p_t = \frac{\partial L}{\partial \dot{t}} = -E \quad (\text{A2})$$

$$p_\phi = \frac{\partial L}{\partial \dot{\phi}} = L \quad (\text{A3})$$

where we identify the constants of motion as the energy and angular momentum of a test particle.

If we assume motion in the equatorial plane (i.e. $\theta = \pi/2$, $\dot{\theta} = 0$) we can write the relativistic four-momentum (of a massive particle) normalisation as

$$p_t p^t + p_r p^r + p_\phi p^\phi = -m^2 \quad (\text{A4})$$

where m is the mass of a test particle. Using the definitions of the energy and angular momentum of the particle and taking into account that $p^\alpha = \dot{x}^\alpha$, we can rewrite the above equation as

$$-E\dot{t} + L\dot{\phi} + g_{rr}\dot{r}^2 = -m^2. \quad (\text{A5})$$

Now, we can find the expressions for the contravariant momenta p^t and p^ϕ from $p_\alpha = g_{\alpha\beta}p^\beta$

$$p^t = \frac{g_{\phi\phi}E + g_{t\phi}}{g_{t\phi}^2 - g_{tt}g_{\phi\phi}} \quad (\text{A6})$$

$$p^\phi = -\frac{g_{tt}L + g_{t\phi}}{g_{t\phi}^2 - g_{tt}g_{\phi\phi}} \quad (\text{A7})$$

now, we can replace these expressions into Eq. (A4) and write the expression for the radial velocity \dot{r}

$$\dot{r} = \left(-m^2 + \frac{g_{\phi\phi}E^2 + 2g_{t\phi}LE + g_{tt}L^2}{g_{t\phi}^2 - g_{tt}g_{\phi\phi}} \right)^{\frac{1}{2}}. \quad (\text{A8})$$

We want to consider circular orbits, so the radial velocity must be $\dot{r} = 0$. Then, we arrive at

$$g_{t\phi}^2 - g_{tt}g_{\phi\phi} = g_{\phi\phi}e^2 + 2g_{t\phi}le + g_{tt}l^2 \quad (\text{A9})$$

where we have introduced the specific energy per unit mass ($e = E/m$) and the specific angular momentum per unit mass ($l = L/m$). Additionally, we are interested

in bound orbits. Specifically, we want marginally bound orbits ($e = 1$). Taking this into account, we get the following expression for the specific angular momentum

$$l_b^\pm = \frac{g_{t\phi} \pm \sqrt{(g_{t\phi}^2 - g_{tt}g_{\phi\phi})(1 + g_{tt})}}{-g_{tt}} \quad (\text{A10})$$

which corresponds to Eq. (7). It is well-known that in black hole spacetimes there is an innermost circular marginally bound orbit for test particles. Naturally, a marginally bound particle at the innermost circular orbit has to have the smallest possible value of the specific angular momentum (i.e. a minimum of Eq. (A10)). The radial location of said minimum is, obviously, the innermost circular marginally bound radius r_{mb} .